Research Square

Preprints are preliminary reports that have not undergone peer review.
They should not be considered conclusive, used to inform clinical practice,
or referenced by the media as validated information.

Magnetic-Field-Assisted Hydrothermal Synthesis of Rod-Like Fe 3 O 4 : Morphology Evolution and Magnetic Retention under Flow

Hetong Guo
East China University of Science and Technology
Pingping Yao
East China University of Science and Technology
Zhenfen Tian
East China University of Science and Technology
Ansa Khalid
East China University of Science and Technology
Yuxiang Yang
yxyang@ecust.edu.cn
East China University of Science and Technology
Weiwei Huan
Zhejiang A&F University

Research Article

Keywords: magnetic-field-assisted synthesis, Fe3O4 nanorods, shape anisotropy, magnetic properties, magnetic retention under flow

Posted Date: November 20th, 2026

DOI: https://doi.org/10.21203/rs.3.rs-11618726/v1

License: This work is licensed under a Creative Commons Attribution 4.0 International License.
Read Full License

Additional Declarations: No competing interests reported.

Magnetic-Field-Assisted Hydrothermal Synthesis of Rod-Like Fe_3O_4: Morphology Evolution and Magnetic Retention under Flow

HETONG GUO[1] · PINGPING YAO[1] · ZHENFEN TIAN[1] · ANSA KHALID[1] · YUXIANG YANG[1*] · WEIWEI HUAN[2*]

[1] *School of Chemistry and Molecular Engineering, East China University of Science and Technology, Shanghai 200237, China*

[2] *College of Chemistry and Materials Engineering, Zhejiang A&F University, Hangzhou 311300, China*

*Corresponding author: Yuxiang Yang, e-mail: yxyang@ecust.edu.cn

*Corresponding author: Weiwei Huan, e-mail: huanweiwei@zafu.edu.cn

Abstract

An external magnetic field can influence the anisotropic growth of magnetic nanocrystals; however, the relationship between field-induced morphology and magnetic retention under flow remains insufficiently understood. In this study, Fe_3O_4 was synthesized hydrothermally under a magnetic field of 0.36 T (F-Fe_3O_4) and under otherwise identical zero-field conditions (Z-Fe_3O_4). The effects of NaOH dosage, reaction time, and temperature on product formation were investigated, and the resulting samples were characterized in terms of crystal structure, morphology, and magnetic properties. Both samples retained the magnetite crystal structure. F-Fe_3O_4 exhibited a rod-like morphology, with a length of approximately 75 nm and a width of approximately 25 nm. HRTEM analysis indicated that F-Fe_3O_4 grew along the easy magnetization axis [110]. In contrast, Z-Fe_3O_4 consisted of irregular polygonal and spherical particles with diameters of 12-18 nm. Increasing the NaOH dosage promoted particle elongation, whereas shorter reaction times and higher temperatures suppressed rod formation. F-Fe_3O_4 exhibited a discontinuity near 270 K, attributed to the Verwey transition, and a saturation magnetization of 54.2 emu g^{-1},compared with 106.3 emu g^{-1} for Z-Fe_3O_4. After silica coating, the saturation magnetization of F-Fe_3O_4@SiO_2 was 20.39 emu g^{-1}. In a flowing-water model under an external magnetic field, the retention rates of F-Fe_3O_4, Z-Fe_3O_4, and F-Fe_3O_4@SiO_2 were 68.43%, 66.09%, and 52.18%, respectively. These results establish a relationship between magnetic-field-assisted morphology evolution, magnetic properties, and magnetic retention under flow.

Keywords: magnetic-field-assisted synthesis; Fe_3O_4 nanorods; shape anisotropy; magnetic properties; magnetic retention under flow

Introduction

Magnetite (Fe_3O_4) nanomaterials possess an inverse spinel structure and respond readily to external magnetic fields. Their magnetic behavior depends on particle crystallinity,

size, morphology, and surface state (Ma et al. 2023; Castellanos-Rubio et al. 2021). Morphology-controlled synthesis has yielded Fe_3O_4 nanorods, nanowires, and assembled chains. In these one-dimensional forms, aspect ratio and geometric anisotropy influence hysteresis and field response (Sugumaran et al. 2021). Precursor chemistry and reaction pathways also shape the size and morphology of Fe_3O_4 nanocrystals (Qiao et al. 2017; Feld et al. 2019). Their macroscopic magnetic response reflects the combined contributions of magnetocrystalline anisotropy, shape anisotropy, surface effects, and interparticle interactions (Ma et al. 2023). Tracking morphology evolution together with magnetic measurements provides a basis for examining how rod-like anisotropy relates to the magnetic behavior of Fe_3O_4.

An external magnetic field can influence the orientation and assembly of magnetic particles. Preformed Fe_3O_4 hybrid nanorods can undergo oriented assembly in a magnetic field, but this post-synthesis rearrangement differs from field-assisted crystal formation (Ye et al. 2023). Earlier studies reported magnetic-field-induced hydrothermal growth of Fe_3O_4 nanowires (Wang et al. 2004) and magnetic-field-assisted reverse coprecipitation of Fe_3O_4 nanorods (Zhang et al. 2011). Shibaev et al. (2020) further showed that pH and OH^- concentration alter iron-oxide precipitation under a magnetic field, producing rod-like or nearly spherical particles . These studies show that both the applied field and the reaction environment influence one-dimensional Fe_3O_4 formation. The combined relationships among field-assisted and zero-field growth, reaction-condition-dependent morphology evolution, and magnetic response remain insufficiently resolved within a matched hydrothermal system. Magnetic-field-induced orientation and dipolar interactions may act alongside solution chemistry and reaction kinetics, and their relative contributions are expected to vary with the synthesis conditions.

Surface and interface control after anisotropic Fe_3O_4 formation can further influence particle dispersion and behavior in an applied field. SiO_2 shells can improve the colloidal stability of magnetic particles and provide readily functionalized surfaces (Zou et al. 2025). Controlled SiO_2 shells have been constructed on anisotropic magnetic nanostructures (Nemec and Kralj 2021). In single-crystalline Fe_3O_4 nanorods, coating conditions also affect aggregation and the retention of magnetic properties (Künnecke et al. 2026). Direction-dependent behavior reported for Fe_3O_4@SiO_2 nanorods further illustrates the interaction of these core-shell structures with external magnetic fields (Li et al. 2024). Comparing uncoated and SiO_2-coated rod-like Fe_3O_4 extends this structure-property analysis to interface effects and magnetic retention under flow.

Here, we compare a 0.36 T magnetic-field-assisted hydrothermal synthesis with an otherwise identical zero-field control to examine the relationship between the applied field and anisotropic Fe_3O_4 formation. The products are denoted F-Fe_3O_4 and Z-Fe_3O_4, respectively. We vary NaOH dosage, reaction time, and temperature to track morphology evolution under field-assisted conditions and relate the structural observations to magnetic measurements. We then coat F-Fe_3O_4 with SiO_2 to produce F-Fe_3O_4@SiO_2 and assess the accompanying changes in core-shell structure and magnetic parameters. Finally, we compare the three materials in a flowing system to evaluate their magnetic retention under an external field. These experiments examine field-assisted formation and morphology evolution, then compare the magnetic behavior and retention under flow of the zero-field, field-assisted, and SiO_2-coated products.

Experimental

Reaction device

The ring-shaped high-temperature magnetic field source, customized by Shanghai Jieling Magnetic Equipment Co., Ltd., can generate a parallel magnetic field of 0.36 T at

temperatures up to 280 ℃. A 25 mL reactor can be placed in its central opening to provide a stable parallel magnetic field during the reaction, as shown in Fig. 1a, b.

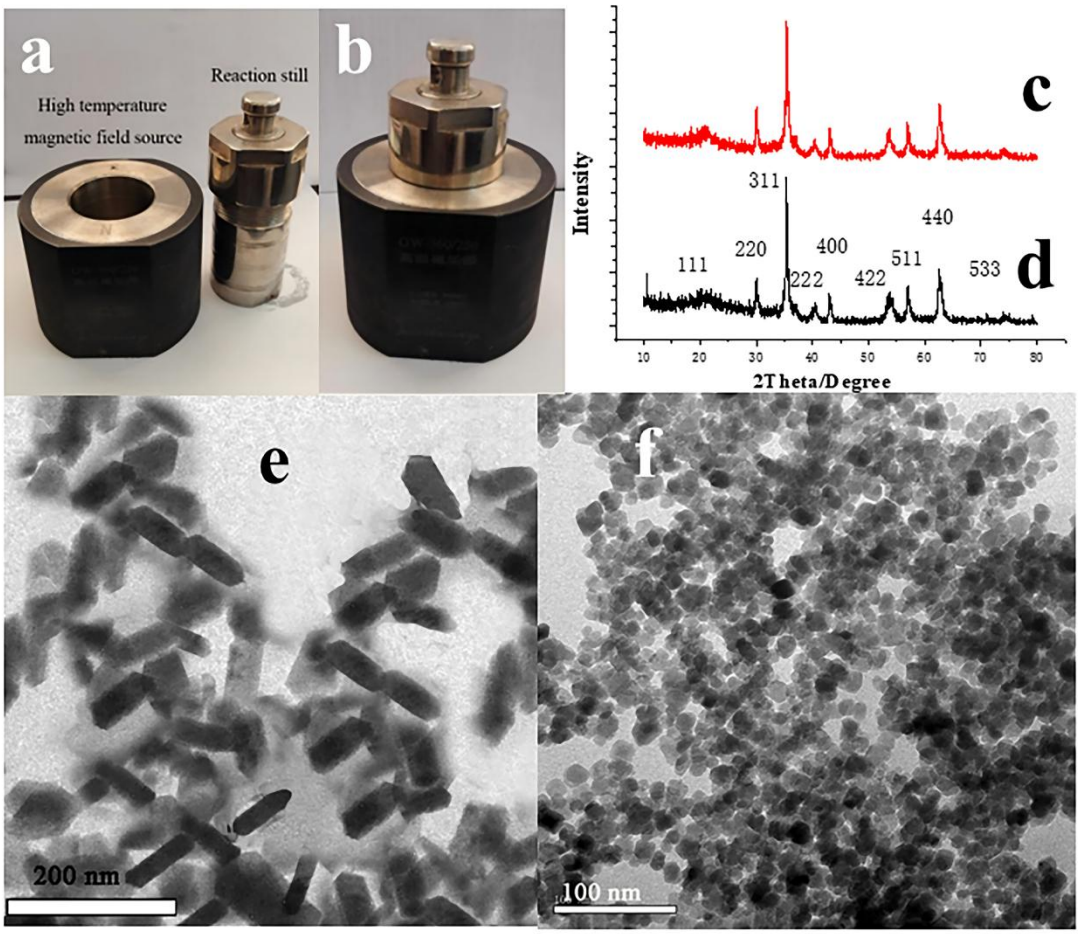

Fig. 1 (a, b) Reactor used for hydrothermal synthesis under a magnetic field; (c) XRD pattern of F-Fe_3O_4 prepared under a magnetic field; (d) XRD pattern of Z-Fe_3O_4 prepared without a magnetic field; (e) TEM image of F-Fe_3O_4; (f) TEM image of Z-Fe_3O_4

Preparation of rod-shaped Fe_3O_4 by hydrothermal method

First, a 0.1 mol/L $FeCl_2$ solution was prepared using nitrogen-saturated twice-distilled water, and 15 mL was placed in a 250 mL round-bottom flask. NaOH (0.3 g) was dissolved in 2.5 mL of $H_4N_2{\cdot}H_2O$ (50%), and the solution was slowly added to the $FeCl_2$ solution under mechanical stirring at 30 ℃ for 15 min. The entire process was conducted under nitrogen protection. The resulting solution was transferred to a polytetrafluoroethylene-lined autoclave, placed in a 0.36 T magnetic field, and heated at 130 ℃ for 6 h. After cooling to room

temperature, the product was washed three times with deionized water and anhydrous ethanol and vacuum-dried at 45 °C for 12 h to obtain a black product denoted F-Fe_3O_4.

For comparison, Z-Fe_3O_4 nanoparticles were prepared under zero-field conditions, with all other reaction parameters unchanged.

Preparation of Fe_3O_4@SiO_2

F-Fe_3O_4 was coated with silica using the classical Stöber method. First, 50 mg of F-Fe_3O_4 nanoparticles was dispersed in 20 mL of deionized water by sonication for 30 min and transferred to a 250 mL round-bottom flask. Anhydrous ethanol (80 mL), concentrated ammonia solution (2.0 mL, 28 wt%), and tetraethyl orthosilicate (TEOS, 1 mL) were then added, and the mixture was mechanically stirred overnight at 30 ℃. The reaction mixture changed from dark black to light gray, consistent with silica coating of the magnetic particles. The light-gray product was magnetically separated, washed three times with deionized water and anhydrous ethanol, and dried in a vacuum oven to obtain F-Fe_3O_4@SiO_2.

Determination of iron content in Fe_3O_4 magnetic fluid

Iron standard solutions with concentrations of 0.02, 0.04, 0.06, 0.08, and 0.10 g/L were prepared. Their absorbance values were measured spectrophotometrically and used to construct a calibration curve of absorbance (A) versus iron concentration (C).

A 1 mL aliquot of magnetic fluid was diluted to 100 mL, and 25 mL of the diluted sample was transferred to a 50 mL colorimetric tube. Hydrochloric acid (5 mL) and hydroxylamine hydrochloride solution (1 mL) were added, and the mixture was heated in a boiling-water bath for 20 min. After cooling, phenanthroline solution (2 mL) and ammonium acetate buffer solution (5 mL) were added. The mixture was diluted to the calibration mark with water, mixed, and allowed to stand for 10 min. Absorbance was then measured against a reagent blank at 510 nm using a 3 cm cuvette, and the iron concentration was calculated from the calibration equation.

Study on simulated magnetic targeting in vitro

An in vitro flowing-water model was used to simulate magnetic targeting because the corresponding physical quantities are difficult to measure accurately in vivo. Fe_3O_4 nanoparticles and glass tubes were used to represent magnetic particles and blood vessels, respectively. The magnetic field was supplied by a YMC-11 medical pulse magnetic field generator. Particle accumulation under the applied magnetic field was observed, and the corresponding measurements were recorded.

Fig. 2 shows the experimental setup for simulated magnetic targeting in vitro. F is a horizontally placed glass tube with a diameter of 3.8 mm, and spherical region G has a radius of 3 mm and serves as the target area. The enlarged target area was used to facilitate observation of particle accumulation and to simulate magnetic-field-driven migration toward surrounding tissue. Fe_3O_4 nanoparticles were dispersed in distilled water, and the suspension was allowed to stand for 1 h before use. The suspension was then delivered through the glass tube by an adjustable constant-flow pump, while the field was applied from one side using the YMC-11 generator.

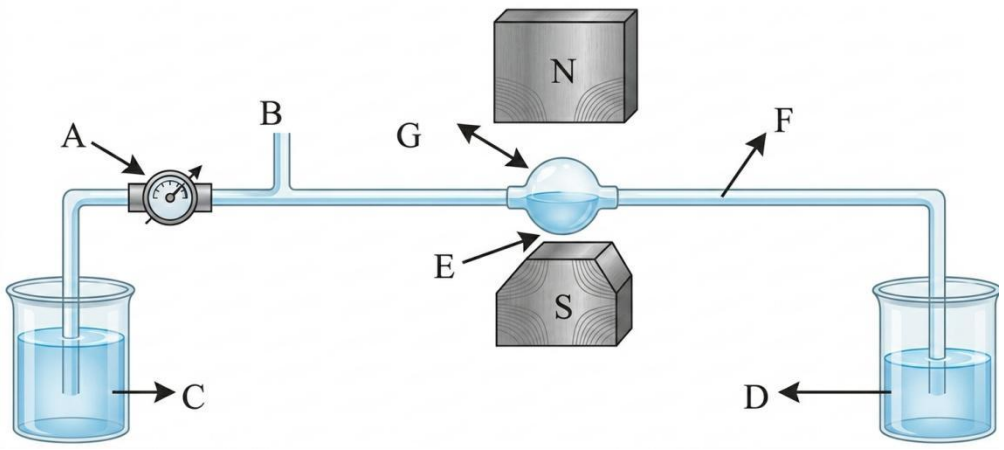

Fig. 2 Experimental diagram of magnetic targeting

In this simulation, 2 mL of magnetic fluid was injected at inlet B, with water as the mobile phase. Pump A was operated at a flow rate of 1.131 mL/min. The magnetic field generator was set to 600 V, and the distance between glass tube F and the magnetic pole was

2 cm. Retention in the magnetic region was observed, and the effluent was collected in container D. The retention rate was calculated as μ (%) = $[1 - (C_2 \times V_2)/(C_1 \times V_1)] \times 100$, where C_2 and V_2 are the iron concentration and volume of the collected effluent, respectively, and C_1 and V_1 are the corresponding values for the magnetic fluid injected at B.

Results and discussion

Analysis of XRD

As shown in Fig. 1c, d, the XRD peak positions of the two Fe_3O_4 samples are largely consistent with the standard Fe_3O_4 pattern (JCPDS No. 19-0629), indicating that the applied magnetic field does not substantially change the characteristic crystal structure and that the products predominantly exhibit the Fe_3O_4 phase.

Analysis of TEM

As shown in Fig. 1e, f, F-Fe_3O_4 exhibits an elongated rod-like morphology, with an average long-axis length of approximately 75 nm and a short-axis length of approximately 25 nm. In contrast, Z-Fe_3O_4 comprises irregular polygonal and spherical particles with diameters of about 12–18 nm. This comparison indicates that the applied magnetic field affects Fe_3O_4 growth and favors the formation of rod-like structures.

Analysis of HRTEM

As shown in Fig. 3a, F-Fe_3O_4 grows in a specific direction. The HRTEM image shows lattice fringes with an interplanar spacing of approximately 0.48 nm, consistent with the (111) planes of Fe_3O_4, indicating that F-Fe_3O_4 grows along the easy magnetization axis [110]. This result agrees with the preceding interpretation.

The response of magnetic nanomaterials to an external magnetic field during synthesis may involve the Lorentz force. This force acts on charged iron species in solution and may affect the nucleation and growth of Fe_3O_4 crystals. Anisotropy in surface tension during crystal growth contributes to the formation of elongated F-Fe_3O_4 rods under a magnetic field,

whereas Fe_3O_4 prepared without a field exhibits irregular polygonal and spherical morphologies. Further in situ observations are required to clarify how the field affects crystal growth. In summary, the applied magnetic field can induce oriented growth of Fe_3O_4 nanocrystals along the easy magnetization axis.

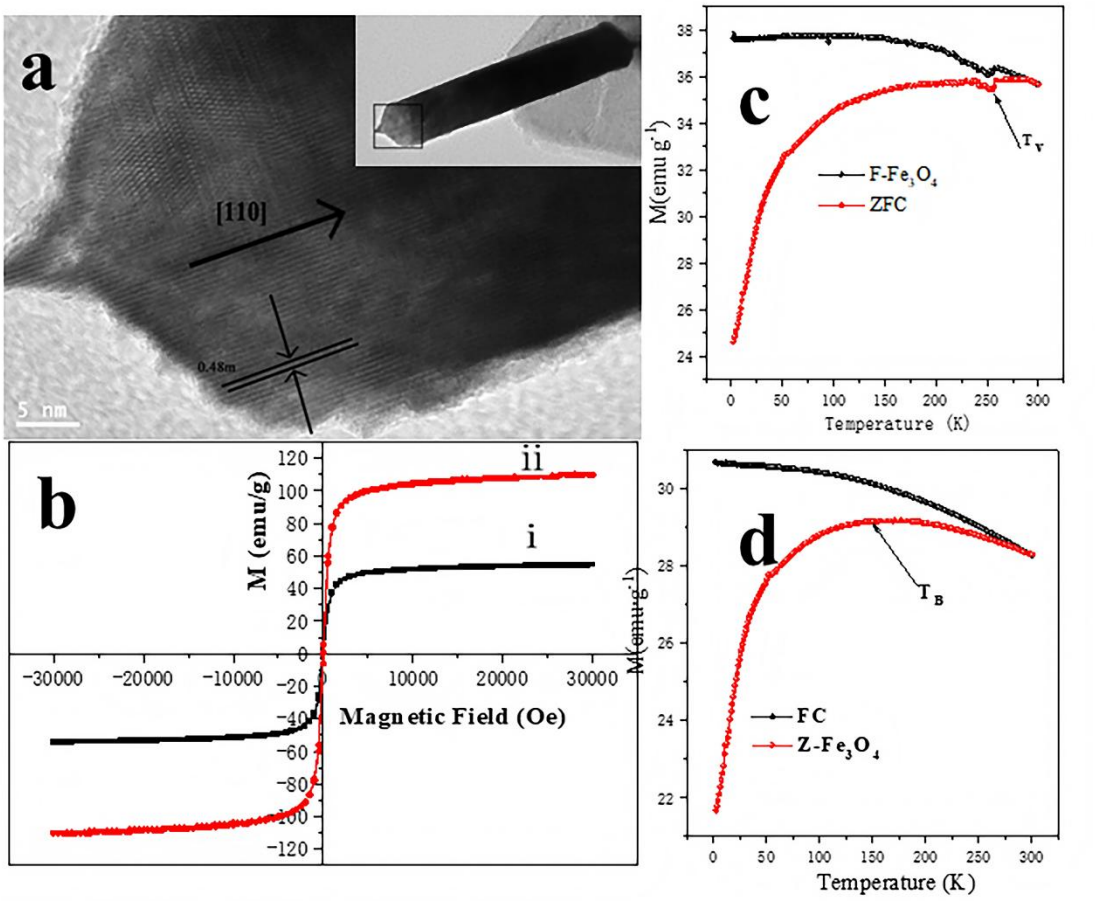

Fig. 3 (a) HRTEM image of F-Fe_3O_4 (rod-like morphology shown in the inset); (b) M–H curves of (i) F-Fe_3O_4 and (ii) Z-Fe_3O_4; (c) ZFC–FC curves of F-Fe_3O_4; (d) ZFC–FC curves of Z-Fe_3O_4

Analysis of magnetic properties

As shown by the M–H curves in Fig. 3b (i, ii), neither Fe_3O_4 sample exhibits an obvious hysteresis loop, indicating superparamagnetic behavior, mainly attributable to the small particle sizes. The saturation magnetization of Z-Fe_3O_4 reaches 106.3 emu g^{-1}, whereas that of F-Fe_3O_4 is 54.2 emu g^{-1}. This difference may arise from the greater shape anisotropy

of F-Fe_3O_4 nanorods. The random orientations of the rods lead to a smaller net magnetization component along the applied field than that of the nearly spherical, isotropic Z-Fe_3O_4 particles. Moreover, because F-Fe_3O_4 nanorods grow along the easy magnetization axis [110], their magnetic domains are aligned in parallel and may be antiparallel to the measurement field. Reorienting these domains along the external field requires overcoming a higher energy barrier, consistent with the subsequent ZFC–FC behavior of F-Fe_3O_4.

As shown in Fig. 3c, the ZFC curve of F-Fe_3O_4 nanorods does not exhibit an obvious blocking temperature (T_B). The temperature-dependent magnetic behavior of nanoparticles is influenced by magnetocrystalline anisotropy, shape anisotropy, surface effects, and interparticle magnetic interactions (Ma et al. 2023). During heating, thermal agitation may facilitate the alignment of initially antiparallel magnetic domains with the applied field, offsetting the instability associated with shape anisotropy. In addition, the ZFC–FC curves of F-Fe_3O_4 show a discontinuous change near 270 K, which corresponds to the Verwey transition region. Thus, 270 K is the Verwey transition temperature (T_V) of F-Fe_3O_4. For bulk Fe_3O_4, T_V is generally approximately 120 K, and the transition is sensitive to stoichiometry, crystallinity, particle size, and surface state (Castellanos-Rubio et al. 2021). The shape anisotropy arising from the rod-like morphology may affect the temperature-dependent magnetization (Ma et al. 2023; Sugumaran et al. 2021). Above T_V, rapid electron hopping occurs between Fe^{2+} and Fe^{3+} at octahedral B sites in the Fe_3O_4 lattice. The higher T_V (270 K) observed for the F-Fe_3O_4 nanorods is mainly attributed to the large magnetic anisotropy energy associated with their rod-like morphology under the applied magnetic field.

As shown in Fig. 3d, the ZFC–FC curve of Z-Fe_3O_4 exhibits a blocking temperature (T_B) near 150 K but no apparent Verwey transition (T_V). This difference indicates that one-dimensional, rod-like magnetic nanomaterials can display magnetic properties distinct from

206 those of approximately isotropic particles. The increase in magnetization with temperature
207 may be of interest for further magnetic applications.

208 **Analysis of the effect of reaction conditions on morphology**

209 The morphology control of nanocrystals is mainly through the following ways:

210 (1) Control the growth rate of nanomaterials in a certain direction, such as the use of
211 different adsorption amounts of surfactants in different crystal faces to inhibit or increase the
212 growth rate of nanomaterials in a specific direction.

213 (2) The intrinsic crystal structure also influences morphology. For example, barium
214 ferrite can form hexagonal nanosheets owing to its hexagonal crystal structure.

215 (3) The synergy of the two effects

216 Hydrazine hydrate has both oxidizing and reducing properties in alkaline solution.
217 Under nitrogen protection, some Fe^{2+} is oxidized to Fe^{3+} by hydrazine hydrate, leading to the
218 gradual formation of Fe_3O_4 under hydrothermal conditions. The reaction is expressed as
219 follows:

220 $$3Fe(OH)_2 + H_4N_2 \xrightarrow{\text{hydrothermal condition}} Fe_3O_4 + 2H_2O + 2NH_3 \qquad (1)$$

221 The slow oxidation involving hydrazine hydrate prolongs the growth of Fe_3O_4,
222 allowing the external magnetic field to act during crystal growth. To infer the field-assisted
223 formation process of nanorods, one reaction parameter was varied at a time while the others
224 were kept constant.

225 *Effect of the amount of NaOH on the morphology of samples*

226 As shown in Fig. 4a, with 0.1 g of NaOH and all other conditions unchanged, the
227 product consists mainly of polygonal particles, approximately 80 nm in size, together with a
228 small proportion of rods. Increasing the NaOH dosage to 0.45 g produces more rod-like
229 particles, with long-axis lengths of approximately 250 nm (Fig. 4b). At 0.6 g, needle-like
230 structures with lengths of 1–1.5 μm appear (Fig. 4c). This may be because NaOH

concentration affects the diffusion rate of Fe^{3+} in the reaction mixture. At a lower NaOH concentration, the lower OH^- concentration and faster diffusion of Fe^{3+} promote more rapid Fe_3O_4 growth, reducing the time available for the magnetic field to affect crystal growth. At a higher NaOH concentration, slower diffusion and growth may permit a stronger field effect, favoring growth along the easy magnetization axis. Some irregular particles also appear at higher NaOH dosage, which is attributed to the formation of an FeOOH phase in the product.

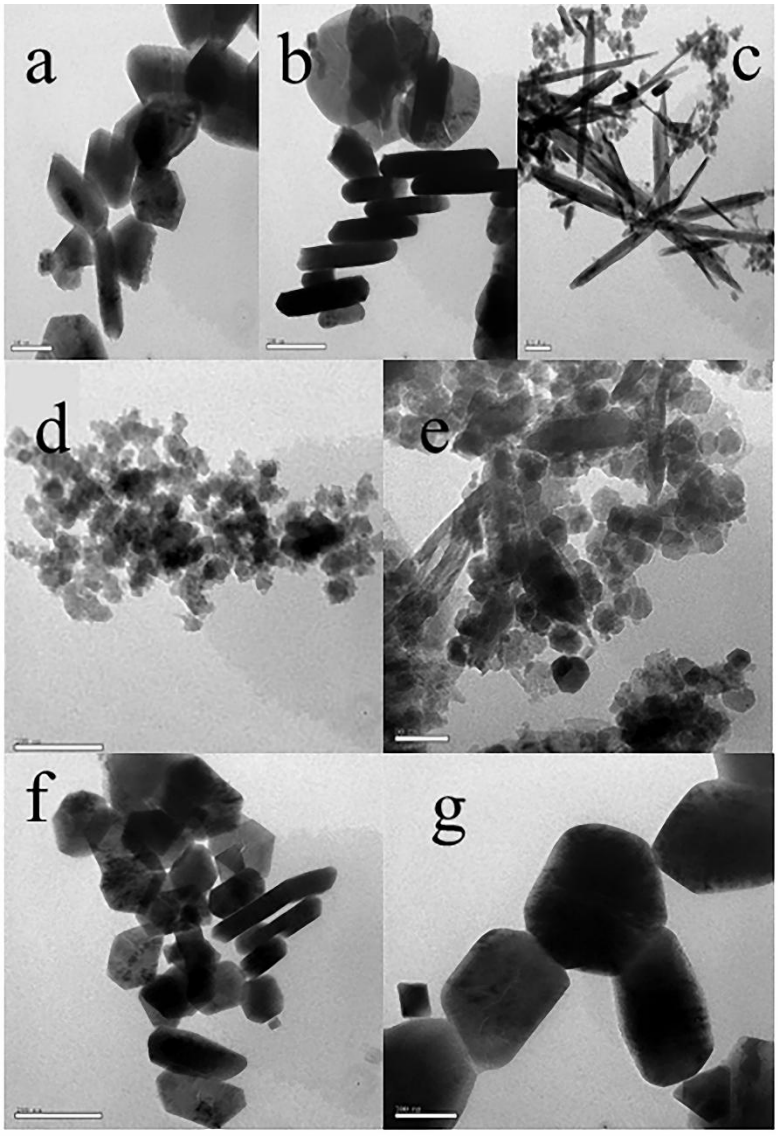

Fig. 4 TEM images of products prepared with different NaOH dosages: (a) 0.1 g, (b) 0.45 g, and (c) 0.6 g; different reaction times: (d) 0.5 h and (e) 3 h; and different reaction temperatures: (f) 160 ℃ and (g) 180 ℃

Effect of reaction time on sample morphology

As shown in Fig. 4d, e, after 0.5 h of reaction under the magnetic field, the products are mainly irregular secondary particles. After 3 h, rod-like structures begin to appear. This observation is consistent with the proposed formation of secondary particles at the initial stage, followed by their gradual assembly into rod-like structures under the magnetic field as the reaction proceeds and hydrazine hydrate undergoes slow oxidation.

Effect of reaction temperature on sample morphology

As shown in Fig. 4f, g, the product morphology becomes increasingly irregular and polygonal as the reaction temperature increases. At 160 ℃, a small number of rod-like particles with lengths of 180–200 nm are present; at 180 ℃, the products are mainly irregular polygonal particles of approximately 220 nm. This is attributed to stronger Brownian motion at higher temperatures, which disrupts the anisotropic effect of the applied field and favors aggregation into polygonal particles. The particles are also larger than those synthesized without the magnetic field.

Analysis of the effect of silica coating

To facilitate potential biological applications, the prepared rod-like Fe_3O_4 was coated with SiO_2 (Fig. 5). As shown in Fig. 5a, some particles exhibit a core–shell structure, although noticeable aggregation is also observed. In Fig. 5b, a broad diffraction feature appears near 20°, consistent with amorphous silica, while the other diffraction peaks correspond to characteristic Fe_3O_4 reflections.

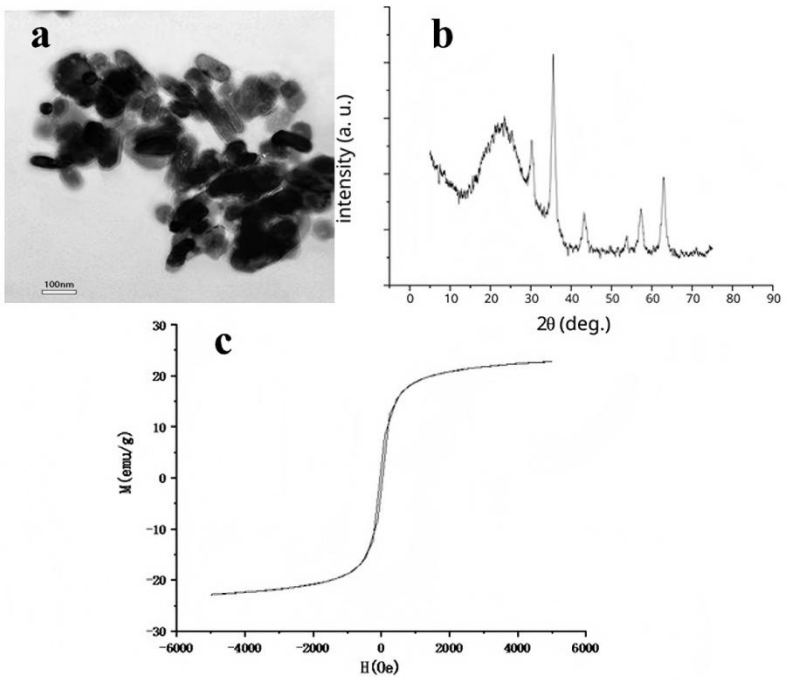

Fig. 5 (a) TEM image, (b) XRD pattern, and (c) M–H curve of SiO_2-coated rod-like Fe_3O_4

As shown in Fig. 5c, the saturation magnetization (M_s) of Fe_3O_4@SiO_2 is 20.39 emu g^{-1}, its remanent magnetization (M_r) is 2.13 emu g^{-1}, and its coercivity (H_c) is 36.62 Oe. These values indicate that the SiO_2-coated Fe_3O_4 particles retain a measurable magnetic response. Together with the TEM and XRD results, they support the formation of SiO_2-coated magnetic particles, although some aggregation is present.

Analysis of simulated magnetic targeting in vitro

The three samples were compared in a simulated in vitro magnetic-targeting experiment. Iron concentrations were determined by the phenanthroline colorimetric method. Standard solutions containing 0.02, 0.04, 0.06, 0.08, and 0.10 g/L Fe were prepared as described in Section 2.4. Absorbance at 510 nm was plotted against iron concentration to obtain a calibration curve. Linear regression yielded $Y = -0.0017 + 1.365X$ ($R^2 = 0.9999$), where Y is absorbance and X is iron concentration in g/L. The concentrations C_1 and C_2 obtained from the calibration equation were used to calculate the retention rate as $\mu\ (\%) = [1 - (C_2 \times V_2)/(C_1 \times V_1)] \times 100$.

As shown in Table 1(a), Z-Fe_3O_4 has a higher saturation magnetization (106.3 emu g^{-1}) but a lower retention rate (66.09%) than F-Fe_3O_4 (54.2 emu g^{-1} and 68.43%, respectively). The slightly higher retention of F-Fe_3O_4 may be associated with its rod-like morphology and differences in suspension behavior. A possible contribution is the viscosity associated with particle–fluid interactions, which may influence particle movement and accumulation even at a controlled pump flow rate. Particle size and volume fraction can affect suspension viscosity. Therefore, despite its lower saturation magnetization, F-Fe_3O_4 exhibits a somewhat higher retention rate of 68.43% under the tested conditions.

F-Fe_3O_4@SiO_2 exhibits the lowest saturation magnetization of the three samples and a retention rate of 52.18%.

The effects of magnetic-pole distance and pulse voltage on magnetic-fluid retention are summarized in Table 1(b). At a pole distance of 2 cm, increasing the pulse voltage from 500 to 600 and 700 V increases the magnetic field strength and raises the retention rate from 67.78% to 70.70% and 83.69%, respectively. At 500 V, increasing the pole distance from 2 to 10 cm decreases retention from 67.78% to 59.63%.

Table 1. Magnetic fluid retention rates for different particle types and magnetic field conditions

(a) Retention rate of magnetic fluid of different samples

Number	Sample	M_s (emu g^{-1})	C_1 (g/L)	C_2 (g/L)	Retention rate (%)
1	Z-Fe_3O_4	106.3	3.03	0.0822	66.09
2	F-Fe_3O_4	54.2	3.12	0.0788	68.43
3	F-Fe_3O_4@SiO_2	20.39	2.81	0.1075	52.18

(b) Retention of magnetic fluid under different conditions

Number	Pulse parameter (V)	Magnetic pole distance (cm)	Magnetic field peak (mT)	C_2 (g/L)	Retention rate (%)
1	500	2	277	0.0786	67.78
2	500	10	54	0.0985	59.63
3	600	2	380	0.0715	70.70
4	700	2	435	0.0398	83.69

These results show that magnetic particles accumulate in the test region under the pulsed magnetic field, with retention rates above 50% under the investigated conditions. Retention increases with pulse voltage at a fixed pole distance and decreases as the distance from the magnetic pole increases. The findings provide preliminary experimental data for future magnetic-targeting studies.

Conclusions

The main findings on magnetic-field-assisted synthesis of Fe_3O_4 and Fe_3O_4@SiO_2 and their simulated in vitro magnetic retention are summarized as follows:

(1) Fe_3O_4 nanorods with a long axis of approximately 75 nm and a short axis of approximately 25 nm were successfully prepared by hydrothermal synthesis under an external magnetic field. The nanorods grow along the easy magnetization axis [110]. Their saturation magnetization reaches 54.2 emu g^{-1} owing to their characteristic shape anisotropy. The magnetization of F-Fe_3O_4 changes with temperature, and a Verwey transition temperature

(T_V) of 270 K is observed. The applied magnetic field therefore influences both the morphology and magnetic properties of Fe_3O_4.

(2) The effects of NaOH dosage, reaction temperature, and reaction time on particle morphology were investigated. The field-assisted formation process of one-dimensional magnetic nanomaterials was discussed, providing a basis for further studies of magnetic-field-directed growth.

(3) Rod-like Fe_3O_4 was coated with SiO_2 to facilitate further surface modification and potential applications.

(4) Under the pulsed magnetic field, the materials exhibited accumulation and retention rates above 50% in the flowing-water model. These observations provide experimental support for further investigations of magnetic targeting.

Statements and Declarations

Funding

No funding was received for conducting this study.

Competing Interests

The authors declare no competing interests.

Author Contributions

H.G. conceived the study, developed the methodology, and wrote the original manuscript draft. P.Y. performed the formal analysis. Z.T. conducted the investigation. W.H. carried out the validation and supervised the research. A.K. and Y.Y. reviewed and edited the manuscript. Y.Y. also supervised the research. All authors reviewed and approved the final manuscript.

Data Availability

The datasets generated and/or analyzed during the current study are available from the corresponding authors upon reasonable request.

References

Castellanos-Rubio I, Arriortua O, Iglesias-Rojas D, Barón A, Rodrigo I, Marcano L, Garitaonandia JS, Orue I, Fdez-Gubieda ML, Insausti M (2021) A milestone in the chemical synthesis of Fe_3O_4 nanoparticles: unreported bulklike properties lead to a remarkable magnetic hyperthermia. Chem Mater 33:8693–8704. https://doi.org/10.1021/acs.chemmater.1c02654

Feld A, Weimer A, Kornowski A, Winckelmans N, Merkl JP, Kloust H, Zierold R, Schmidtke C, Schotten T, Riedner M, Bals S, Weller H (2019) Chemistry of shape-controlled iron oxide nanocrystal formation. ACS Nano 13:152–162. https://doi.org/10.1021/acsnano.8b05032

Künnecke NJ, Morales I, Schaefer MA, Polarz S (2026) Insights into growing silica around monocrystalline magnetite nanorods leading to colloids with improved magnetic properties—obstacles and solutions. Nanomaterials 16:219. https://doi.org/10.3390/nano16030219

Li C, Chen Z, Xiao M, Liu J, Huang Y, Zhu Z, Liu Y, Pan L, An X, Hua W, He L (2024) Magneto-photonic effect of Fe_3O_4@SiO_2 nanorods for visualizing the direction of magnetic fields with high spatiotemporal resolution. ACS Appl Mater Interfaces 16:70656–70664. https://doi.org/10.1021/acsami.4c16841

Ma Z, Mohapatra J, Wei K, Liu JP, Sun S (2023) Magnetic nanoparticles: synthesis, anisotropy, and applications. Chem Rev 123:3904–3943. https://doi.org/10.1021/acs.chemrev.1c00860

Nemec S, Kralj S (2021) A versatile interfacial coassembly method for fabrication of tunable silica shells with radially aligned dual mesopores on diverse magnetic core nanoparticles. ACS Appl Mater Interfaces 13:1883–1894. https://doi.org/10.1021/acsami.0c17863

Qiao L, Fu Z, Li J, Ghosen J, Zeng M, Stebbins J, Prasad PN, Swihart MT (2017) Standardizing size- and shape-controlled synthesis of monodisperse magnetite (Fe_3O_4) nanocrystals by identifying and exploiting effects of organic impurities. ACS Nano 11:6370–6381. https://doi.org/10.1021/acsnano.7b02752

Shibaev AV, Shvets PV, Kessel DE, Kamyshinsky RA, Orekhov AS, Abramchuk SS, Khokhlov AR, Philippova OE (2020) Magnetic-field-assisted synthesis of anisotropic iron oxide particles: effect of pH. Beilstein J Nanotechnol 11:1230–1241. https://doi.org/10.3762/bjnano.11.107

Sugumaran PJ, Yang Y, Wang Y, Liu X, Ding J (2021) Influence of the aspect ratio of iron oxide nanorods on hysteresis-loss-mediated magnetic hyperthermia. ACS Appl Bio Mater 4:4809–4820. https://doi.org/10.1021/acsabm.1c00040

Wang J, Chen Q, Zeng C, Hou B (2004) Magnetic-field-induced growth of single-crystalline Fe_3O_4 nanowires. Adv Mater 16:137–140. https://doi.org/10.1002/adma.200306136

Ye Z, Li Z, Feng J, Wu C, Fan Q, Chen C, Chen J, Yin Y (2023) Dual-responsive Fe_3O_4@polyaniline chiral superstructures for information encryption. ACS Nano 17:18517–18524. https://doi.org/10.1021/acsnano.3c06461

Zhang W, Jia S, Wu Q, Ran J, Wu S, Liu Y (2011) Convenient synthesis of anisotropic Fe_3O_4 nanorods by reverse co-precipitation method with magnetic field-assisted. Mater Lett 65:1973–1975. https://doi.org/10.1016/j.matlet.2011.03.101

Zou Y, Sun Z, Wang Q, Ju Y, Sun N, Yue Q, Deng Y, Liu S, Yang S, Wang Z, Li F, Hou Y, Deng C, Ling D, Deng Y (2025) Core–shell magnetic particles: tailored synthesis and applications. Chem Rev 125:972–1048. https://doi.org/10.1021/acs.chemrev.4c00710